Instability and "Pearling" States Produced in Tubular Membranes by Competition of Curvature and Tension

Roy Bar-Ziv and Elisha Moses
Department of Physics of Complex Systems, Weizmann Institute of Science, Rehovot 76100, Israel
(Received 19 April 1994)

We investigate the stability of tubular fluid membranes by perturbing them with optical tweezers. A peristaltic instability appears, with wavelength on the order of the tube circumference, characterized by tautness and suppression of curvature fluctuations in the membrane. We interpret this in terms of a model that includes a surface tension term in the elastic energy, and describes a transition to stable, finite amplitude peristaltic states. At high amplitudes the experiment reveals new dynamic states of "pearls" interconnected via thin tubes along which they travel and aggregate.

PACS numbers: 68.10.–m, 02.40.–k, 47.20.–k, 87.22.Bt

Stability of the cylindrical geometry is one of the most basic and instructive hydrodynamic issues. As discovered by Savart [1], a cylinder of fluid is unstable and breaks up into droplets. This forms the basis for everyday phenomena such as the drops on a spider's web, and has numerous technological applications, e.g., the coating of thin wires [2]. The instability's origin was shown to be surface tension by Plateau [3], who noticed that for wavelengths larger than a cylinder's circumference, oscillatory ("peristaltic") perturbation of the cylinder can reduce the surface area while retaining its volume. This problem first prompted Rayleigh [4] to investigate issues of the most unstable wavelength, since in practice the experiment was showing selection of a unique wavelength longer than the circumference. This system is by now a paradigm for similar instabilities in fields like plasma physics and astrophysics [5].

In this Letter we consider stability of membrane tubes, in which the question of surface tension is subtle and delicate. Membranes are usually described by a Helfrich curvature energy [6] (which stabilizes tubes) while surface tension energy is assumed negligible. As predicted [7] and elegantly demonstrated experimentally [8], there are two contributions to membrane tension. Bare compressibility, in which stretching at the molecular level gives a linear ratio of excess area to tension, is energetically very unfavorable. However, thermal curvature fluctuations produce roughness and "fold up" the membrane at all scales, giving an entropic contribution to the tension: "unfolding" the membrane by tension (e.g., by pulling on it) arrests these fluctuations and gives an excess area that is logarithmic with tension. In this way geometric forms with high volume to surface ratio (e.g., spherical vesicles) can store tension but still have the same area per molecule as a fluctuating, floppy vesicle.

Our experimental setup is by now standard [9,10] combining an Ar laser with a phase contrast microscope (63×, 1.4 N.A. objective) to form a trap of diameter ~ 0.3 μm. We used DGDG and DMPC (Sigma) lipid bilayers, with reported [8] bending moduli $\kappa = 0.4 \times 10^{-12}$ and 0.6×10^{-12} erg, respectively, under standard protocol [11,12] with no prehydration. Hydration was performed at high temperature (~ 45 °C) under an induced flow. In this way tubes a few hundred μm long and oriented along the flow are randomly formed. The tubes are anchored at both ends at massive lipid globules typically 10 μm in diameter. Tube radii R_0 of about 0.3 to 5 μm were observed comprising of one or two bilayers [13]. The existence of membrane tubes is an interesting issue on its own [14].

Figure 1 characterizes the initial stages of the instability. The tube [Fig. 1(a)] is stable (over many hours) before application of the tweezers, its thermal fluctuations visibly evident. The application of the tweezers [Fig. 1(b)] for typical times of 0.2–2 sec and using from 20 to 60 mW (increasing with radius R_0) initiates a sinusoidal instability which develops [Fig. 1(c)] to a finite amplitude peristaltic state with a visible reduction in fluctuations. The instability propagates out in both directions from the point of application of the tweezers at a constant velocity. We could measure the outward propagation velocity v in smaller tubes only, measuring velocities between 10 and 70 μm/sec, with 30 μm/sec typical. The natural velocity scale for propagation of a

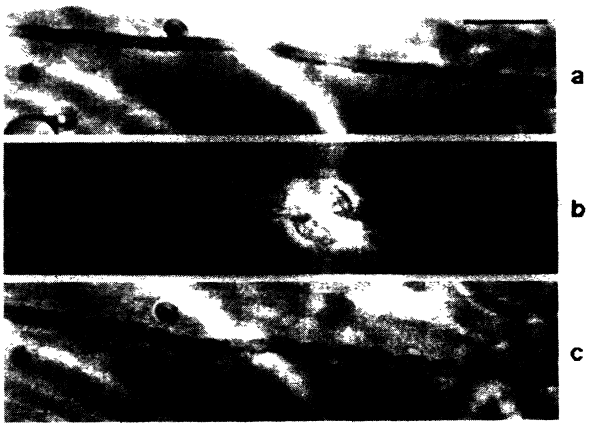

FIG. 1. (a) Section of DMPC tube. (b) Initial instability upon tweezing. Tweezers marked by the circular reflection. State (c) eventually decays to state (a). Bar is 10 μm.

0031-9007/94/73(10)/1392(4)$06.00

curvature mode in a medium with viscosity η is $v_\kappa = \kappa/\eta R_0^2$ which for DMPC in water at 40 °C and with $R_0 = 1$ μm gives $v_\kappa = 100$ μm/sec. Similarly, for surface tension the velocity scale is $v_\sigma = \sigma/\eta$ and the measured propagation velocity $v = 30\mu$m/sec would require $\sigma = v\eta \sim 0.2 \times 10^{-4}$ erg/cm^2. This may be compared to molecular compressibility values [8] of $\sim 10^2$ erg/cm^2.

The suppression of fluctuations [8,16] along with the existence of the well known capillary (Rayleigh) instability of cylinders hints at the existence of a surface tension σ competing with the curvature. To understand the combined effect of surface tension and curvature we look at the energy

$$F = \kappa \int 2H^2 dS + \sigma \int dS. \tag{1}$$

Based on the experiment and on the analysis for the Rayleigh instability [5] we limit ourselves to surfaces that are axisymmetric and in which the axis is unperturbed. For a surface given in parametric form by $G(z, \phi, \rho) \equiv \rho - R(z) = 0$ in axisymmetric cylindrical coordinates the area element is $dS = 2\pi R\sqrt{1 + R_z^2}$. The mean curvature H is [16]

$$H = \frac{RR_{zz} - 1 - R_z^2}{2R(1 + R_z^2)^{3/2}}. \tag{2}$$

We introduce the nondimensional variable $x = qR_0$ and the normalized ratio of surface tension to curvature $s = \sigma R_0^2/\kappa$ as our control parameter, with R_0 the unperturbed tube radius as before. We restrict ourselves here to analysis of sinusoidal perturbations of the form $R(z) = \rho_0 + \epsilon \sin(qz)$. Volume conservation is introduced through the constraint $\rho_0 = R_0\sqrt{1 - \epsilon^2/2R_0^2}$.

Defining $f(s, x, \epsilon)$ the energy difference per unit length between the peristaltic and straight cylinder, we evaluated $f(\epsilon)$ numerically for different values of s and x, and found for $x < 1$ a transition from the stable cylinder at low s to a new finite amplitude peristaltic state in which curvature balances the destabilizing surface tension. The model gives the transition at $s_c(x) \approx 4$ for $x = 0.8$, giving for σ a value on the order of $4\kappa/R_0^2 \approx 2 \times 10^{-4}$ erg/cm^2. At these small tensions ($\ll 0.5$ dyn/cm) we expect [8] σ to be dominated by entropic contributions from the constraint of curvature fluctuations. An even smaller amount of tension must already exist just to keep the tube anchored at its ends.

The transition is shown in Figs. 2(a) and 2(b) for s values close to s_c. For low values of s all values of x give $f(\epsilon) > 0$. As s increases a band of x opens up for which $f(\epsilon)$ becomes negative and has a minimum at a finite ϵ. The transition can be first [Fig. 1(a)] or second [Fig. 1(b)] order, with a tricritical point at $s \approx 4$ and $x \approx 0.785$. As $s \to \infty$ we recoup the classical Rayleigh instability, where $f(\epsilon)$ decreases monotonically with ϵ for $x < 1$.

To study the model analytically we expand the energy in orders of ϵ. To order ϵ^2 we identify the band of unstable wavelengths whose width expands from 0 to 1 as s increases from 0 to ∞. The new peristaltic states become apparent when we consider terms up to order ϵ^6 (odd powers vanish upon integration over a wavelength, details will be given elsewhere [13]).

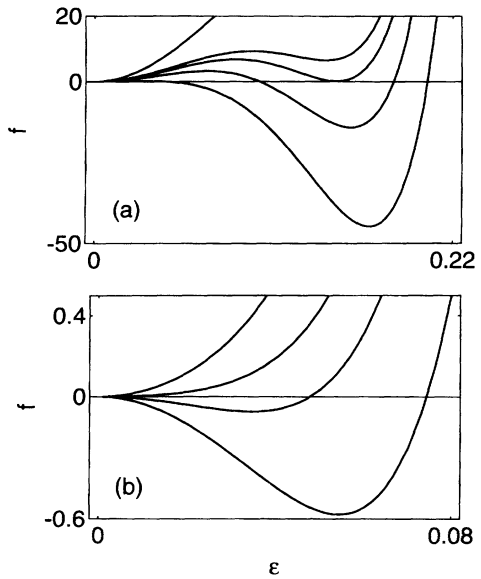

FIG. 2. Excess energy per unit length f in units of $10^{-6}\kappa/R_0$. (a) $x = qR_0 = 0.79$. A first order transition from top to bottom: $s = 4.19$, straight tube stable; 4.1933, straight stable, peristaltic metastable; 4.1937, straight and peristaltic modes in equilibrium; 4.1945, peristaltic stable, straight metastable; 4.196, peristaltic stable. (b) $x = 0.78$. A second order transition from top to bottom: $s = 3.985, 3.9988, 3.999$, and 3.9993.

The phase diagram defined by this Landau-type expansion is shown in Fig. 3 for the relevant wave numbers $0 < x < 1$. In the limit of small s (curvature dominated) the straight cylinder is stable to perturbations of all wavelengths. For $s \to \infty$ we regain the absolute instability driven by surface tension. The lower line defines a transition from the straight cylinder to a sinusoidal peristaltic stable state, which is second order for long wavelength ($x < 0.785$) and first order for $0.785 < x < 1$. The model predicts a limited band of s for which the sinusoidal instability appears. The amplitude of the stable state increases with s, approaching the cylinder radius at the top line. This bounds the region of applicability of the model and beyond it we expect pearls to form. Above (below) the first order transition line is a region (thin lines) where the straight (peristaltic) cylinder is metastable with respect to the peristaltic (straight) one.

Similar to the Rayleigh instability, energy considerations alone do not predict the most unstable wavelength. To do that requires a linear stability analysis of the flow induced in the cylinder. Comparing to the experiment, we note that the wave number in Fig. 1(b) is $x = 0.82$, while in Fig. 1(c) it is slightly larger than 1. This indicates that we are already bordering on the pearling stage, which is described below.

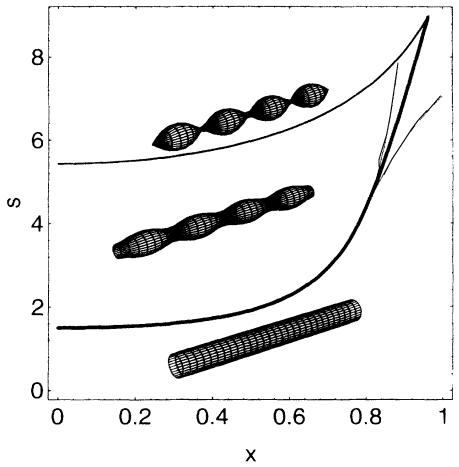

FIG. 3. Stability diagram in the x, s plane. Bottom bold line is the instability line. Thin lines denote regions of metastability. Above the top line the model is no longer adequate and we expect a pearling state to evolve.

We now turn to longer or stronger application of the tweezers in the experiment, which leads to the pearling state shown in Figs. 4 and 5. "Pearls on a string" are produced, isolated spheres that are interconnected by regions that have collapsed to very thin tubes (0.1 − 0.3 μm radius, depending on R_0). These spheres (Fig. 4) travel along the tube towards the point of application of the tweezers, aggregating there. They bring with them excess volume and surface, leaving behind them thin tubes. The velocities for DMPC are typically 0.1 − 10 μm/sec and decay as $V = V_0 e^{-at}$, with $a = 0.02$ sec^{-1} and $V_0 = 5$ μm/sec (but our measurement does not rule out a constant discrete decrement of the velocity every time a pearl reaches the central cluster, a process that approximates an exponential decay in time). The spheres are taut as they move, all fluctuations damped by the surface tension. Note that in the decay of the pearling state (described below) pearls lose this tautness, and we find it significant that floppy pearls do not travel.

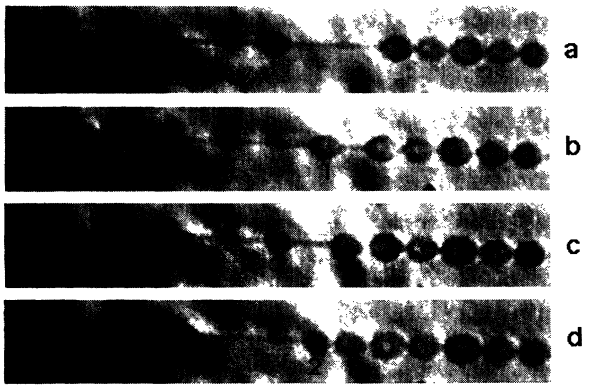

FIG. 4. Pearls moving on a string—nonlinear, late stages of an $R_0 = 1$ μm DMPC tube. Time between frames is 2 sec, starting about 20 sec after the laser was shut off. Bar is 10 μm.

The motion of the pearls indicates [17] a velocity scale v_p set by the Poiseuille flow of water in the very thin tubes which the motion of the pearls causes, $v_p = R_1^2 \vec{\nabla} P / 4\eta$ with $\vec{\nabla} P$ the pressure gradient and R_1 the thin tube radius. Taking as a rough estimate $\vec{\nabla} P \sim \sigma / R_1 L$, the Laplace pressure difference between pearl and tube over a typical distance L between pearls and with $s = \sigma R_0^2 / \kappa$ we obtain $v_p \approx s \kappa R_1 / \eta L R_0^2$. Using $s = 10$ and from Fig. 4: $R_0 = 1.5$ μm, $R_1 = 0.2$ μm, $L = 13$ μm gives v_p on the order of 1 μm/sec, in reasonable agreement with the measured velocities.

It is instructive to study the relaxation of the pearling state and the subsequent release of tension. When the tweezers are released the sinusoidal state of Fig. 1 decays immediately back to the straight cylinder (on the time scale of a second). The pearling state, however, lasts over many minutes, as shown in Fig. 5, where an especially large tube was chosen to demonstrate the structures. In such tubes the linear sinusoidal stage is skipped and the initial stages are irregular, probably because the trap size is smaller than the wavelength. The surface tension is most apparent close to the point of application of the tweezers [Fig. 5(c)], both geometrically and because fluctuations are absent. Once the tweezers are turned off, tension is not immediately released. Its slow release is limited by the water that has to flow through the minuscule passages between the spheres, apparent in Fig. 5(c), which are below our 0.2 μm resolution.

Figures 5(d)–5(f) shows the late stage of the relaxation and coarsening of the structure in a region where the

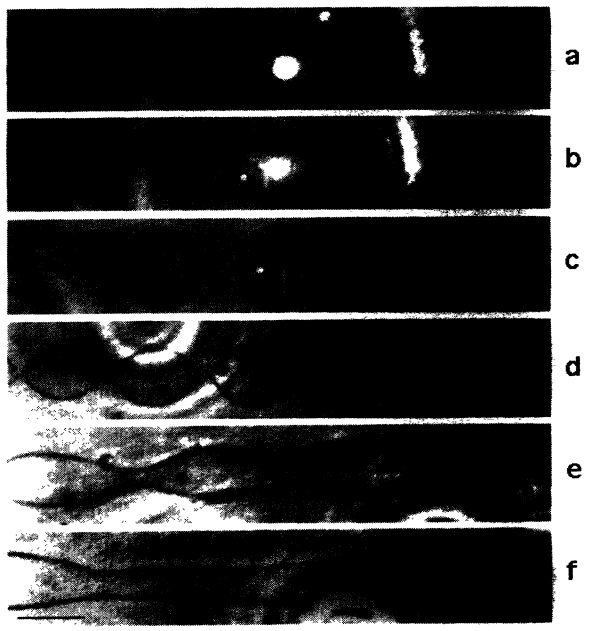

FIG. 5. Time development and relaxation of instability. (a) $t = 0$, application of the tweezers (= bright spot) onto a fluctuating DMPC tube (b) $t = 9$ sec, (c) $t = 30$ sec, tweezers off. (d)–(f) are 100 μm away from (a)–(c). (d) $t = 223$ sec, (e) $t = 577$ sec, and (f) $t = 754$ sec. Bar is 10 μm.

structure is periodic. In Fig. 5(d) production of typical necks between the pearls is apparent. Recent work [18] has shown the necks to be minimal surfaces, thus stable. The pearls are floppy at this stage, with reduced tension. Coarsening typically occurs through the formation of two wavelengths from three.

The limit $s \to \infty$ can be reached experimentally by very high intensity or prolonged application of the tweezers. Indeed, we found that in this way we could splice the tubes at the point of application. Note that reaching high values like $s = 100$, where the Rayleigh instability dominates, still leaves the tension $\sigma \sim 10^{-2}$ erg/cm^2 very small compared to the molecular compressibility. Furthermore, for a finite closed tube moderate application of the tweezers produces a breakup into isolated spheres. We attribute this to the limited surface area—even a small change in area yields high values of s.

Full elucidation of the action of the tweezers on the membrane is a central and intriguing issue which is, however, beyond us at this stage. The Ar laser produces locally both heating and strong electric field gradients, and we cannot conclusively determine which is repsonsible for the effect observed. Heating can produce surface tension changes in a monolayer [20] and shape transformations in vesicles [12]. However, because the membrane's thickness is at the molecular level, the absorbing volume is mostly water and heating should be small [10] (<1 °C). A strong uniform electric field was shown to cause tension [19] and formation of pores ("electroporation") [21] which are essential in some shape transformations [12]. We believe the main action of the tweezers to be pulling of lipid into the trap, with some subsequent loss of surface to the solution [13].

There are additional mechanisms which produce peristaltic shapes in tubes. Deuling and Helfrich [22] showed that spontaneous curvature leads to a peristaltic mode with finite wave number. Bruinsma [23] has pointed out that van der Waals forces would also tend to destabilize cylinders. Pearling occurs when polymers are anchored onto the membrane by hydrophobic side groups [26]. This was explained by a spontaneous curvature, but an interesting possibility is that the polymers actually arrest fluctuations and thus induce tension. Mechanical stress, e.g., by a microtubule growing in the vesicle [24] or a latex bead embedded in the vesicle wall and pulled by optical tweezers [25], also causes pearling of tubular outgrowths.

To summarize, in our picture surface tension is created by the local action of the tweezers. In a cylindrical geometry the long range instability of the membrane tube can be separated from the local, complex effect of the laser. Our model for the energy indicates that even a small tension, well within the entropic regime, suffices to set off the instability. As a result curvature and tension compete to form peristaltic modes and dynamic pearling states in membrane tubes.

We acknowledge useful discussions with F. Brochard, N. Dan, J.-P. Eckmann, R. Granek, V. Lebedev, and R. Zeitak, and an especially fruitful interaction with P. Nelson and S. Safran.

[1] F. Savart, Ann. D. Chim. **53**, 337 (1833).
[2] D. Quere, J.-M. di Meglio, and F. Brochard-Wyart, Science **249**, 1256 (1990).
[3] J. Plateau, *Statique Experimentale et Theorique des Liquides Soumis aux Seules Forces Moleculaires* (Gautier-Villars, Paris, 1873).
[4] Lord Rayleigh, *Scientific Papers* (Dover, New York, 1964), Vol. 1 , pp. 361–371, and 379–401.
[5] S. Chandrasekhar, *Hydrodynamic and Hydromagnetic Stability* (Clarendon Press, Oxford, 1961).
[6] W. Helfrich, Z. Naturforsch **28c**, 693 (1973).
[7] W. Helfrich and R.-M. Servuss, Nuovo Cimento **3**, 137 (1984).
[8] E. Evans and W. Rawicz, Phys. Rev. Lett. **64**, 2094 (1990); M. Bloom, E. Evans, and O. G. Mouritsen, Quart. Rev. Biophys. **24**, 293 (1991).
[9] A. Ashkin, Phys. Rev. Lett. **24**, 156 (1970); Science **210**, 1081 (1980); A. Ashkin, J. M. Dziedzic, and T. Yamane, Nature (London) **330**, 769 (1987).
[10] S. M. Block, in *Noninvasive Techniques in Cell Biology* (Wiley-Liss, New York, 1990), pp. 375–402.
[11] D. Needham and E. Evans, Biochemistry **27**, 8261 (1988); M. Mutz and W. Helfrich, J. Phys. (Paris) **51**, 991 (1990).
[12] J. Kas and E. Sackmann, Biophys. J. **60**, 825 (1991).
[13] R. Bar-Ziv and E. Moses (to be published).
[14] See, e.g., A. S. Rudolph, B. R. Ratna, and B. Kahn, Nature (London) **352**, 52 (1991); P. Nelson and T. Powers, Phys. Rev. Lett. **69**, 3409 (1992); J. V. Selinger and J. M. Schnur, Phys. Rev. Lett. **71**, 4091 (1993).
[15] S. A. Safran, *Statistical Thermodynamics of Surfaces, Interfaces and Membranes* (Addison-Wesley, Reading, MA, 1994).
[16] F. Brochard and J. F. Lennon, J. Phys. **36**, 1035 (1975).
[17] We thank R. Zeitak for pointing this out.
[18] X. Michalet, D. Bensimon, and B. Fourcade, Phys. Rev. Lett. **72**, 168 (1994).
[19] M. Kummrow and W. Helfrich, Phys. Rev. A **44**, 8356 (1991).
[20] M. Wang *et al.*, Phys. Rev. Lett. **71**, 4003 (1993).
[21] Y. Rosenberg and R. Kornstein, Biophys. J. **58**, 823 (1990).
[22] H. J. Deuling and W. Helfrich, Blood Cells **3**, 713 (1977); See also Ou-Yang Zhong-can and W. Helfrich, Phys. Rev. A **39**, 5280 (1989); Miao *et al.*, Phys. Rev. A **43**, 6843 (1991).
[23] R. Bruinsma, J. Phys. (Paris), Colloq. **51**, C7-53 (1990).
[24] D. Fygenson and A. J. Libchaber (private communication).
[25] M. I. Angelova, G. Martinot-Lagarde, and B. Pouligny (to be published).
[26] G. Decher *et al.*, Angew. Makromol. Chem. **166/167**, 71 (1989).

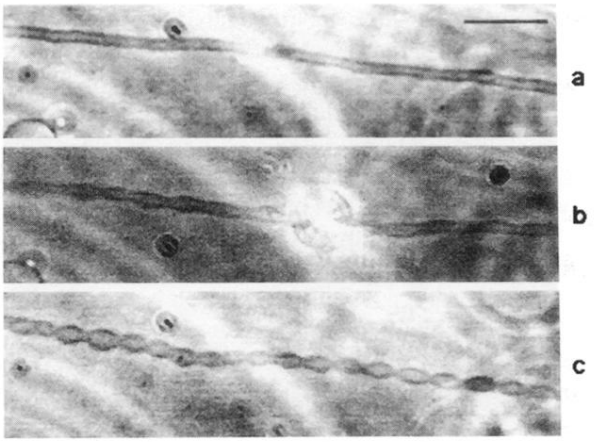

FIG. 1. (a) Section of DMPC tube. (b) Initial instability upon tweezing. Tweezers marked by the circular reflection. State (c) eventually decays to state (a). Bar is 10 μm.

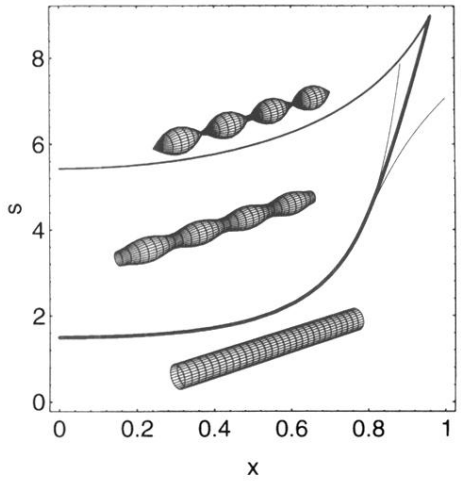

FIG. 3. Stability diagram in the x, s plane. Bottom bold line is the instability line. Thin lines denote regions of metastability. Above the top line the model is no longer adequate and we expect a pearling state to evolve.

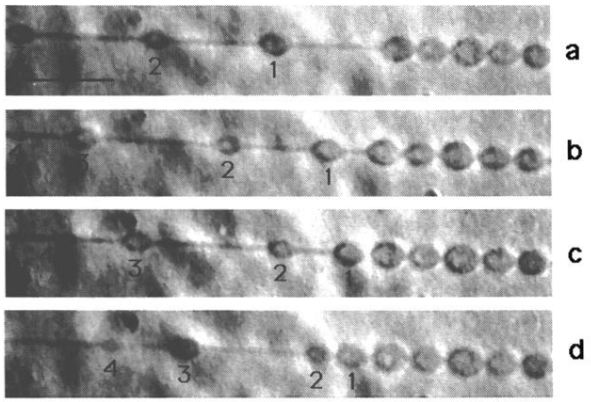

FIG. 4. Pearls moving on a string—nonlinear, late stages of an $R_0 = 1$ μm DMPC tube. Time between frames is 2 sec, starting about 20 sec after the laser was shut off. Bar is 10 μm.

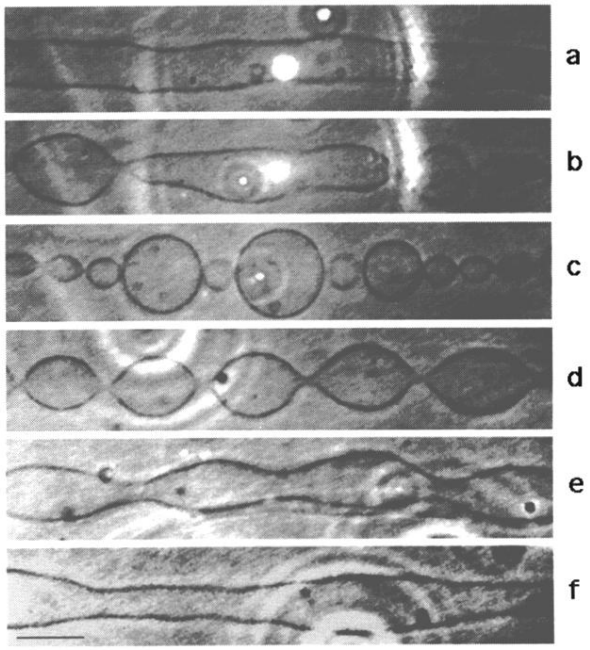

FIG. 5. Time development and relaxation of instability. (a) $t = 0$, application of the tweezers (= bright spot) onto a fluctuating DMPC tube (b) $t = 9$ sec, (c) $t = 30$ sec, tweezers off. (d)–(f) are 100 μm away from (a)–(c). (d) $t = 223$ sec, (e) $t = 577$ sec, and (f) $t = 754$ sec. Bar is 10 μm.